Contents lists available at Science-Gate

International Journal of Advanced and Applied Sciences

Journal homepage: http://www.science-gate.com/IJAAS.html

Gravitational influences on micropolar blood flow in a bifurcated artery with mild stenosis

Yan Bin Tan [1,*], Norzieha Mustapha [2]

[1]Faculty of Computing and Information Technology, Tunku Abdul Rahman University College, Jalan Genting Klang, Setapak, Kuala Lumpur, Malaysia
[2]Faculty of Computer and Mathematical Sciences, Universiti Teknologi MARA Kelantan, Bukit Ilmu, Machang, Kelantan, Malaysia

ARTICLE INFO

Article history:
Received 5 February 2018
Received in revised form
20 August 2018
Accepted 1 September 2018

Keywords:
Bifurcated artery
Blood flow
Gravity
Micropolar fluid
Stenosis

ABSTRACT

A finite difference approach has been implemented to study blood flow in a bifurcated artery with a single mild stenosis under the effects of gravitational force. Streaming blood along the vessel segment is assumed to be micropolar, incompressible, laminar, unsteady and fully-developed. Geometry of the blood vessel is modelled as a finite bifurcation. An unsteady two-dimensional nonlinear model is taken where the governing equations are considered together with significant gravity term. The governing equations are solved using Matlab programming. Axial velocities and some blood flow characteristics are obtained and presented in graphical form. From the results, increment of dimensionless gravity parameter value yields lower axial velocity along the bifurcation segment, as well as higher magnitude of outer wall shear stress and lower magnitude of inner wall shear stress. At the branching junction, distortion happens which could lead to various consequences such as multiple stenosis. While gravity term is considered in the study, increment of viscosity yields lower axial velocity and wall shear stress along the vessel segment. These show that gravitational acceleration term and the branching structure are two substantial components to be considered in blood flow model.

1. Introduction

Cardiovascular disease has been noticed as one of the major illnesses around the world. Common cardiovascular diseases such as hypertension, angina, stroke, vessel thrombosis and so on are often related to abnormality, disorder and malfunction of blood vessel. Among the illnesses occurring through blood vessels, constriction in artery has been found to be one of the most significant factors. This segmental narrowing is developed in inner lining of vessel walls by arterial plaque, which is usually made up of deposits of fatty substance, cholesterol, calcium, fibrin or other cellular waste products. As a result, blood clots or thrombosis would form. Blood functions as a system of transportation, regulation and protection in human body. This situation then leads to abnormal flowing of blood, hence affect function of blood as protection, transportation and regulation in human body. Also, this kind of unhealthy deposition or stenosis in a vessel tends to raise blood pressure and reduce vessel elasticity. Due to inadequate blood supplement, infected part of the body will get numbness. More seriously, stroke may occur if the blood supply is cut off to the brain. Furthermore, this abnormality of blood flow would probably cause the present stenosis to further get worse by forming additional constrictions and coupling effects (Ku, 1997). Hence, numerous medical studies have been carried out to further understand cardiovascular blood flow and stenosis in blood vessels.

Blood used to be modelled as Newtonian and non-Newtonian fluid by adopting several justifiable assumptions. Chakravarty et al. (1996) pointed out that blood behaves as Newtonian fluid when it flows through wider arteries such as the aorta; and oppositely, non-Newtonian behaviours are observed in tinier arteries. Eringen (1966) introduced a theory of a specialised non-Newtonian fluid, namely the micropolar fluid, which considers the involvement of micro-structure, to model and describe some kind of fluid suspensions. While blood is a composition of various particles such as erythrocytes, leukocytes, thrombocytes, plasma, and other carried substances, it is sufficient to be categorised as a kind of

* Corresponding Author.
Email Address: tanyb@tarc.edu.my (Y. B. Tan)
https://doi.org/10.21833/ijaas.2018.11.003

suspension. Micropolar fluid model considers the natural characteristics of blood compound suspension where each blood particle can affect the flow (Lukaszewicz, 1999). These mathematical bio-mechanical studies have provided remarkable and extensive advancement in the field of cardiology (Ariman et al., 1973; Devanathan and Parvathamma, 1983; Ghosh, 1986; Muthu et al., 2003; Abdullah and Amin, 2010; Ikbal et al., 2011; Chakravarty and Mandal, 2013). Despite, in current clinical field, constrictions and abnormal behaviours of blood in vessel is still commonly observed using various invasive methods. Thus, persistency in mathematical modelling of blood flow and stenosis is important to give deeper understanding on blood flow rheology, and provide more ideas on the hemodynamic. One can even able to speculate the cause of some common phenomena such as stenosis overlapping and restenosis by investigating the blood flow characteristics.

On the other hand, gravitational force is one of the fundamental forces regulating biological and physiological systems. From previous researches, it is interesting to find out that gravitational acceleration does not only differ on earth and in space. On the earth itself, different altitude and latitude will give different values of gravity acceleration (Payne, 2004). Also, during postural changes, blood assembles at certain part of body because of gravity attraction, and this will lead to increment of blood pressure at that body part (Olufsen et al., 2005). However, not many of the previous studies included gravity as a body force in modelling blood flow in arteries, thus this becomes the main motivation to this research. Throughout this research, variation of gravitational acceleration is taken into consideration to provide deeper insight about its effects on blood flow in constricted arteries (Burrowes and Tawhai, 2006; Burrowes et al., 2005).

Apart from quantitative factors such as gravity force, physical factors such as vessel structures are also found to be one of the major factors affecting blood flow behaviour in human cardiovascular system (Lou and Yang, 1993). Blood vessels are a series of branches expanding throughout the body, therefore bifurcation structure is very common among the branching system (Chakravarty and Mandal, 1997). This kind of structure has been clinically proven to be significant on atherogenesis, which means the augmentation of arterial wall deposition. This phenomenon is also clearly remarked where clinical investigations point out that arterial stenosis often occurs at bifurcated vessel regions. Due to this, branching structures have become one of the interested and important aspects in modelling blood flow to find out properties of flow rheology passing through vessel bifurcations (Shaw et al., 2009; Tan et al., 2014). In this current research, blood flow is modelled as micropolar fluid and its effects when passing through an artery bifurcation under variation of gravity acceleration is investigated.

Despite researches about blood flow in living body have been carried out since decades, characteristics of blood flow in cardiovascular system has not yet been developed and interpreted thoroughly. This is because apart from quantitative parameters, too many subjective factors are affecting behaviours of human anatomy, including environment and even the internal individual emotions. However from the angle of mathematical modelling, even though a lot of assumptions need to be made, such analyses progressively give larger picture to successfully relate to clinical circumstances. Thus, this study formulates problem regarding the effects of gravitational acceleration, structure of bifurcated artery, involvement of a single stenosis at the parent branch, and modelling of blood flow as micropolar fluids. The finite difference method is used in this study; while streaming blood is assumed to be two-dimensional, laminar, time-dependent, and fully-developed.

2. Geometry profile

The geometry model of this study is a segment of bifurcated artery with a single mild stenosis occurred at parent branch. This model was first established by Chakravarty and Mandal (1997), where axisymmetric segment of artery is assumed to be made up of finite straight circular cylinders. In this study, geometry of the bifurcation segment is set to be dimensionless, and is described mathematically by Eq. 1 and Eq. 2 below. Eq. 1 is the function of $R_1(z)$ while Eq. 2 is the function $R_2(z)$, which are piecewise functions in terms of z, describing radii geometries of outer vessel wall and inner vessel wall respectively. Illustration of the geometry profile is shown in Fig. 1.

Here, a and r_1 are the non-constricted (non-stenotic region) radii of the parent and daughter branches respectively. Curvatures are introduced at each junction of the bifurcation segment. This is to ensure the continuity of flow such that non-existent flow separations can be avoided. r_0 and r_0' are the radii of curvatures for the lateral junction and flow divider respectively. Besides, l_0 is stenosis length; d' denotes the segment length from the axial origin to the stenosis; θ is the angle of bifurcated branch horizontally; τ_m is the maximum height of the stenosis.

$$\begin{cases} 1 & , 0 \le z \le d' \\ 1 - \frac{4\tau_m}{a l_0^2}[l_0(z-d') - (z-d')^2] & , d' \le z \le d' + l_0 \\ 1 & , \ d' + l_0 \le z \le z_1 \\ 1 + \frac{r_0}{a} - \sqrt{\left(\frac{r_0}{a}\right)^2 - (z-z_1)^2} & , \ z_1 \le z \le z_2 \\ \frac{2r_1}{a}\sec\theta + (z-z_2)\tan\theta & , \ z_2 \le z \le z_{max} \end{cases} \quad (1)$$

$$\begin{cases} 0 & , 0 \le z \le z_3 \\ \sqrt{r_0'^2 - (z - z_3 - r_0')} & , z_3 \le z \le z_3 + r_0'(1-\sin\theta) \\ r_0'\cos\theta + z_4 & , z_3 + r_0'(1-\theta) \le z \le z_{max} \end{cases} \quad (2)$$

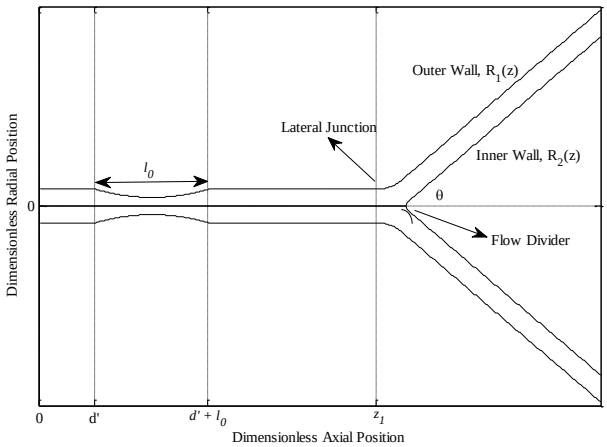

Fig. 1: Geometry profile

Along the z-axis, z_1 is the starting point of the lateral junction, z_2 is the ending point of the lateral branching junction, z_3 is the apex, and z_{max} denotes the finite length of the segment. Further, parameters comprised in the above geometry (1) and (2) are defined as follows:

$$z_2 = z_1 + \left(1 - \frac{2r_1}{a}\sec\theta\right)\frac{\sin\theta}{\cos\alpha - 1} \quad (3)$$

$$z_3 = z_2 + q \quad (4)$$

$$z_4 = [z - z_3 - r_0'(1 - \sin\theta)]\tan\theta \quad (5)$$

$$r_0 = \frac{a - 2r_1\sec\theta}{\cos\theta - 1} \quad (6)$$

$$r_0' = (z_0 - z_2)\frac{\sin\theta}{1 - \sin\theta} \quad (7)$$

with the choice of $q = 0.3$, where q is the distance from z_2 to the bifurcated apex lying between 0.1 and 0.5. Furthermore, $R_1(z)$ and $R_2(z)$ are denoted to be time-dependent. Hence, the time-variant geometry profile is given by multiplying $R_1(z)$ and $R_2(z)$ with respective periodic functions of time, $a_1(t)$ and $b_1(t)$ as shown below, to describe the wall motion, such that $R_1(z,t) = R_1(z) \cdot a_1(t)$, $R_2(z,t) = R_2(z) \cdot b_1(t)$.

$$a_1(t) = 1 - (\cos\omega t - 1)ke^{-k\omega t} \quad (8)$$

$$b_1(t) = 1/a_1(t) \quad (9)$$

here, k is a constant; $\omega = 2\pi f_p$ is the angular frequency in which f_p is the pulse frequency equals 1.2Hz.

3. Governing equations

In this study, streaming blood that passes through the segment of artery bifurcation is considered to have suspended rigid and non-uniform particles described by micropolar fluid model. It is set to be two-dimensional, incompressible, laminar, unsteady, and fully-developed.

The set of equations governed in this study consists of the continuity equation, the radial momentum equation, the axial momentum equation and the angular momentum equation, which are derived from the conservation of mass, conservation of linear momentum and conservation of angular momentum respectively. Conservative forms of the governing equations are:

$$\frac{\partial\tilde{w}}{\partial\tilde{z}} + \frac{\tilde{u}}{\tilde{r}} + \frac{\partial\tilde{u}}{\partial\tilde{r}} = 0 \quad (10)$$

$$\frac{\partial\tilde{u}}{\partial\tilde{t}} + \frac{\partial\tilde{u}^2}{\partial\tilde{r}} + \frac{\partial(\tilde{w}\tilde{u})}{\partial\tilde{z}} + \frac{\tilde{u}^2}{\tilde{r}} = -\frac{1}{\rho}\frac{\partial\tilde{p}}{\partial\tilde{r}} + \frac{\mu+\kappa}{\rho}\left(\frac{\partial^2\tilde{u}}{\partial\tilde{r}^2} + \frac{1}{\tilde{r}}\frac{\partial\tilde{u}}{\partial\tilde{r}} + \frac{\partial^2\tilde{u}}{\partial\tilde{z}^2} - \frac{\tilde{u}}{\tilde{r}^2}\right) + \frac{\kappa}{\rho}\frac{\partial\tilde{\omega}}{\partial\tilde{z}} + g\sin\phi \quad (11)$$

$$\frac{\partial\tilde{w}}{\partial\tilde{t}} + \frac{\partial(\tilde{u}\tilde{w})}{\partial\tilde{r}} + \frac{\partial\tilde{w}^2}{\partial\tilde{z}} + \frac{\tilde{w}\tilde{u}}{\tilde{r}} = -\frac{1}{\rho}\frac{\partial\tilde{p}}{\partial\tilde{z}} + \frac{\mu+\kappa}{\rho}\left(\frac{\partial^2\tilde{w}}{\partial\tilde{r}^2} + \frac{1}{\tilde{r}}\frac{\partial\tilde{w}}{\partial\tilde{r}} + \frac{\partial^2\tilde{w}}{\partial\tilde{z}^2}\right) + \frac{\kappa}{\rho}\left(\frac{\partial\tilde{\omega}}{\partial\tilde{r}} + \frac{\tilde{\omega}}{\tilde{r}}\right) - g\cos\phi \quad (12)$$

$$\rho I\left(\frac{\partial\tilde{\omega}}{\partial\tilde{t}} + \tilde{u}\frac{\partial\tilde{\omega}}{\partial\tilde{r}} + \tilde{w}\frac{\partial\tilde{\omega}}{\partial\tilde{z}}\right) = -\kappa\left(2\tilde{\omega} + \frac{\partial\tilde{w}}{\partial\tilde{r}} - \frac{\partial\tilde{u}}{\partial\tilde{z}}\right) + \gamma\left(\frac{\partial^2\tilde{\omega}}{\partial\tilde{r}^2} + \frac{1}{\tilde{r}}\frac{\partial\tilde{\omega}}{\partial\tilde{r}} - \frac{\tilde{\omega}}{\tilde{r}^2} + \frac{\partial^2\tilde{\omega}}{\partial\tilde{z}^2}\right) \quad (13)$$

Further, as required in the finite difference method, a pressure gradient needs to be defined before proceeding to the next steps. Blood is pulsatile in nature because due to pumping pace of heart. A cycle of heart pumping consists of a systolic phase and a diastolic phase. Systolic phase is where heart contracts and produces high arterial pressure, enabling oxygenated blood to be transferred to each cell; while diastolic phase is the relaxation of heart when arterial pressure is low. This set of actions of heart is represented by a pressure gradient at the axial direction. As suggested by Burton (1966), for human being, the pressure gradient can be well expressed by a cosine function as follow:

$$-\frac{\partial\tilde{p}}{\partial\tilde{z}} = a_0 + a_1\cos\tilde{\omega}_p\tilde{t} \quad (14)$$

In this prescribed pressure gradient, a_0 is the constant component of the pressure gradient, a_1 is the amplitude of the fluctuating pulsatile component (gives rise to the systolic and diastolic pressure), $\omega_p = 2\pi f_p$ with f_p is the pulse frequency.

Non-dimensionalization procedure needs to be carried out to ensure the terms having same dimension which also match with vessel geometry profile. As suggested by Muthu et al. (2003), a parameter ϖ is involved, which represents frequency of the unsteady flow in unit Hertz (cycle per second). Meanwhile, other related dimensionless parameters are introduced to represent the involved viscosity terms, micropolar fluid terms and also the gravity term. The dimensionless representations are listed as below:

$$t = \varpi\tilde{t},\ r = \frac{\tilde{r}}{a},\ z = \frac{\tilde{z}}{a},\ u = \frac{\tilde{u}}{\varpi a},\ w = \frac{\tilde{w}}{\varpi a},$$
$$\omega = \frac{\tilde{\omega}}{\varpi},\ \omega_p = \frac{\tilde{\omega}_p}{\varpi},\ p = \frac{\tilde{p}}{\mu\varpi},\ A_0 = \frac{aa_0}{\mu\varpi},\ A_1 = \frac{aa_1}{\mu\varpi},$$
$$K = \frac{\kappa}{\mu},\ M = \frac{\gamma}{\mu r_0^2},\ J = \frac{I}{a^2},\ \alpha^2 = \frac{a^2\varpi\rho}{\mu},\ G = \frac{g\rho a}{\mu\varpi}$$

After non-dimensionalisation, the dimensionless governing Eq. 10 and Eq. 13 together with the prescribed pressure gradient Eq. 14 are:

$$\frac{\partial w}{\partial z} + \frac{u}{r} + \frac{\partial u}{\partial r} = 0 \quad (15)$$

$$\alpha^2\left(\frac{\partial u}{\partial t} + u\frac{\partial u}{\partial r} + w\frac{\partial u}{\partial z}\right) = -\frac{1}{\rho}\frac{\partial p}{\partial r} + (1+K)\left(\frac{\partial^2 u}{\partial r^2} + \frac{1}{r}\frac{\partial u}{\partial r} + \frac{\partial^2 u}{\partial z^2} - \frac{u}{r^2}\right) + K\left(\frac{\partial\omega}{\partial z}\right) + G\sin\theta \quad (16)$$

$$\alpha^2\left(\frac{\partial w}{\partial t} + u\frac{\partial w}{\partial r} + w\frac{\partial w}{\partial z}\right) = -\frac{1}{\rho}\frac{\partial p}{\partial z} + (1+K)\left(\frac{\partial^2 w}{\partial r^2} + \frac{1}{r}\frac{\partial w}{\partial r} + \frac{\partial^2 w}{\partial r^2}\right) + K\left(\frac{\partial\omega}{\partial r} + \frac{\omega}{r}\right) - G\cos\phi \quad (17)$$

$$\alpha^2 J\left(\frac{\partial\omega}{\partial t}+u\frac{\partial\omega}{\partial r}+w\frac{\partial\omega}{\partial z}\right)=-K\left(2\omega+\frac{\partial w}{\partial r}-\frac{\partial u}{\partial z}\right)+ M\left(\frac{\partial^2\omega}{\partial r^2}+\frac{1}{r}\frac{\partial\omega}{\partial r}-\frac{\omega}{r^2}+\frac{\partial^2\omega}{\partial z^2}\right) \quad (18)$$

$$-\frac{\partial p}{\partial z}=A_0+A_1\cos\omega_p t \quad (19)$$

4. Initial and boundary conditions

The initial and boundary conditions are adapted from Abdullah and Amin (2010), and Chakravarty and Sen (2005) to fit the current model. Initially, no flow takes place when the system is at rest hence:

$$u(r,z,0)=w(r,z,0)=\omega(r,z,0)=0 \quad (20)$$

The vessel is considered to be axisymmetric in this study. No radial flow takes place along the longitudinal axis of the parent branch. Also, velocity gradient of blood flow is assumed to be zero, which means no shear rate at this segment.

$$u(r,z,t)=\frac{\partial w(r,z,t)}{\partial r}=0 \text{ on } r=0 \text{ for } 0\le z\le z_3 \quad (21)$$

At the wall surface throughout the bifurcation segment, the common axial velocity no-slip condition is applied; while the radial velocity is dependent on vessel wall motion as described by Chakravarty and Sen (2005). The following equations described the conditions at the outer and inner walls respectively, in which $\alpha_0=1$ for $z\le z_3$ while $\alpha_0=sec\,\theta$ for $z\ge z_3$.

$$u=\alpha_0\frac{\partial R_1}{\partial t},\ w=0 \text{ on } r=R_1(z,t)\ \forall z \quad (22)$$

$$u=\alpha_0\frac{\partial R_2}{\partial t},\ w=0 \text{ on } r=R_2(z,t) \text{ for } z\ge z_3 \quad (23)$$

5. Method of solution

The governing equations are solved using explicit finite difference method, and are computed in Matlab programming software. However, transformation and discretization procedures need to be carried out before coding. Also, the radial velocity component will be solved analytically and then be implicated in the numerical solution.

5.1. Radial coordinate transformation

Before the governing equations are discretized, radial coordinate transformation is carried out to provide effects of immobilising the vessel walls by transforming radial terms into expressions that contain terms in coordinate x. For the current model of bifurcated vessel which inner and outer walls, radial coordinate transformation is given by

$$x=\frac{r-R_2(z,t)}{R(z,t)} \quad (24)$$

here, $R(z,t)=R_1(z,t)-R_2(z,t)$. The transformed continuity equation, axial momentum and angular momentum equations are as follows:

$$(xR+R_2)\frac{\partial w}{\partial z}-\frac{xR+R_2}{R}\left(x\frac{\partial R}{\partial z}+\frac{\partial R_2}{\partial z}\right)\frac{\partial w}{\partial x}+u+\left(\frac{xR+R_2}{R}\right)\frac{\partial u}{\partial x}=0 \quad (25)$$

$$\frac{\partial w}{\partial t}=-\frac{1}{\alpha^2}\frac{\partial p}{\partial z}+\frac{1}{R}\left[x\frac{\partial R}{\partial t}+\frac{\partial R_2}{\partial t}-u+w\left(x\frac{\partial R}{\partial z}+\frac{\partial R_2}{\partial z}\right)\right]\frac{\partial w}{\partial x}- w\frac{\partial w}{\partial z}+\frac{1+K}{\alpha^2}\left\{\frac{1}{R^2}\left[1+\left(x\frac{\partial R}{\partial z}+\frac{\partial R_2}{\partial z}\right)^2\right]\frac{\partial^2 w}{\partial x^2}-\frac{2}{R}\left(x\frac{\partial R}{\partial z}+ \frac{\partial R_2}{\partial z}\right)\frac{\partial^2 w}{\partial x\partial z}+\frac{\partial^2 w}{\partial z^2}+\frac{1}{R}\left[\frac{1}{xR+R_2}+\frac{2}{R}\left(x\frac{\partial R}{\partial z}+\frac{\partial R_2}{\partial z}\right)\frac{\partial R}{\partial z}- \left(x\frac{\partial^2 R}{\partial z^2}+\frac{\partial^2 R_2}{\partial z^2}\right)\right]\frac{\partial w}{\partial x}\right\}+\frac{K}{\alpha^2}\left(\frac{1}{R}\frac{\partial\omega}{\partial x}+\frac{\omega}{xR+R_2}\right)-G\cos\phi \quad (26)$$

$$\frac{\partial\omega}{\partial t}=\frac{1}{R}\left[x\frac{\partial R}{\partial t}+\frac{\partial R_2}{\partial t}-u+w\left(x\frac{\partial R}{\partial z}+\frac{\partial R_2}{\partial z}\right)\right]\frac{\partial\omega}{\partial x}-w\frac{\partial w}{\partial z}- \frac{K}{\alpha^2 J}\left[2\omega+\frac{1}{R}\frac{\partial w}{\partial x}-\frac{\partial u}{\partial z}+\frac{1}{R}\left(x\frac{\partial R}{\partial z}+\frac{\partial R_2}{\partial z}\right)\frac{\partial u}{\partial x}\right]+\frac{M}{\alpha^2 J}\left\{-\frac{\omega}{(xR+R_2)^2}+ \frac{1}{R^2}\left[1+\left(x\frac{\partial R}{\partial z}+\frac{\partial R_2}{\partial z}\right)^2\right]\frac{\partial^2\omega}{\partial x^2}+\frac{\partial^2\omega}{\partial z^2}-\frac{2}{R}\left(x\frac{\partial R}{\partial z}+\frac{\partial R_2}{\partial z}\right)\frac{\partial^2\omega}{\partial x\partial z}+ \frac{1}{R}\left[\frac{1}{xR+R_2}+\frac{2}{R}\left(x\frac{\partial R}{\partial z}+\frac{\partial R_2}{\partial z}\right)\frac{\partial R}{\partial z}-\left(x\frac{\partial^2 R}{\partial z^2}+\frac{\partial^2 R_2}{\partial z^2}\right)\right]\frac{\partial\omega}{\partial x} \quad (27)$$

At the same time, the boundary conditions (20) – (23) are also transformed to:

$$u(x,z,0)=w(x,z,0)=\omega(x,z,0)=0 \quad (28)$$

$$u(x,z,t)=\frac{\partial w(x,z,t)}{\partial x}=0 \text{ on } x=0 \text{ for } 0\le z\le z_3 \quad (29)$$

$$u(x,z,t)=\alpha_0\frac{\partial R_1}{\partial t},\ w(x,z,t)=0 \text{ on } x=1\ \forall z \quad (30)$$

$$u(x,z,t)=\alpha_0\frac{\partial R_2}{\partial t},\ w(x,z,t)=0 \text{ on } x=0 \text{ for } z\ge z_3 \quad (31)$$

5.2. Radial velocity component

Radial velocity function should be obtained prior to the starting of finite difference algorithm. First of all, from Eq. 25, integration with respect to x from limit 0 to x is performed on both sides. After simplified and rearranged, it becomes

$$u(x,z,t)=\frac{R_2}{xR+R_2}u(0,z,t)+\left(x\frac{\partial R}{\partial z}+\frac{\partial R_2}{\partial z}\right)w(x,z,t)- \frac{R_2}{xR+R_2}\int_0^x\left[(xR+R_2)\frac{\partial w}{\partial z}+\left(2x\frac{\partial R}{\partial z}+\frac{R_2}{R}\frac{\partial R}{\partial z}+\frac{\partial R_2}{\partial z}\right)w\right]dx \quad (32)$$

Then, the integral limits are expanded and boundary conditions are applied. The equation is then simplified and rearranged to become:

$$\int_0^1\left[(xR+R_2)\frac{\partial w}{\partial z}+\left(2x\frac{\partial R}{\partial z}+\frac{R_2}{R}\frac{\partial R}{\partial z}+\frac{\partial R_2}{\partial z}\right)w\right]dx= \frac{R_2}{R}u(0,z,t)-\frac{R_1}{R}\alpha_0\frac{\partial R_1}{\partial t} \quad (33)$$

To equalise the above integrals and integrands, an arbitrary function shall be introduced such that $\int_0^1 f(x)dx=1$ and $f(1)=0$. From Chakravarty and Sen (2005), the function adopted is:

$$f(x)=-4x(x^2-1) \quad (34)$$

Thus, the radial velocity component equation is obtained as below:

$$u(x,z,t)=\frac{R_2}{xR+R_2}u(0,z,t)+\left(x\frac{\partial R}{\partial z}+\frac{\partial R_2}{\partial z}\right)w(x,z,t)+ \frac{x^2(2-x^2)}{xR+R_2}\left[R_1\alpha_0\frac{\partial R_1}{\partial t}-R_2u(0,z,t)\right] \quad (35)$$

5.3. Finite difference scheme

The finite difference expressions for the derivatives are formed by discretization techniques with reference to Taylor's series expansions. The finite difference approximations for velocities here are based on central differencing in uniform

staggered grids; while the time derivative is discretized using first order forward difference approximation. Also, we define $x = j\Delta x$, $z = i\Delta z$ and $t = k\Delta t$ for the bifurcated artery segment under investigation. k refers to the time step, where Δt is the pre-defined time increment. Δx and Δz represent the uniform width (radial direction) and length (axial direction) of any (i, j)-th cell respectively, as shown in Fig. 2.

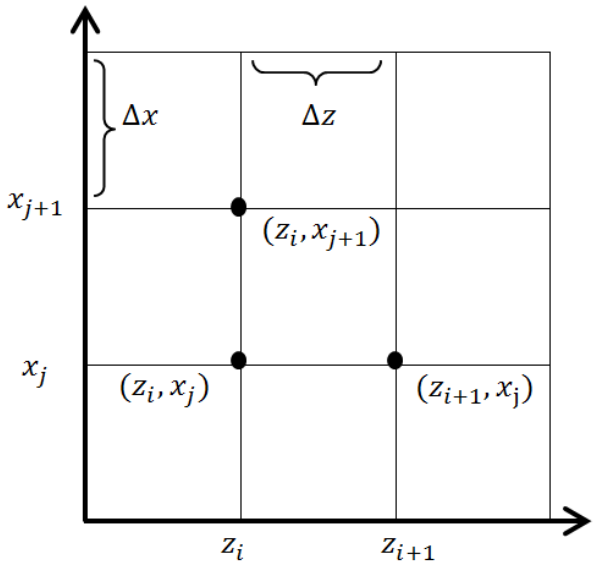

Fig. 2: Finite difference uniform grids

The axial momentum Eq. 26 and angular momentum Eq. 27 are discretized based on central difference approximations for all the spatial derivatives. Likewise, any spatial differential terms regarding the radial velocity u are also discretized similarly to the above approximations. The equations are then rearranged to become:

$$w_{i,j}^{k+1} = w_{i,j}^{k} + \Delta t\{-\frac{1}{\alpha^2}\frac{\partial p}{\partial z} + \frac{1}{R_i^k}\left[x_j\left|\frac{\partial R}{\partial z}\right|_i^k + \left|\frac{\partial R_2}{\partial z}\right|_i^k - u_{i,j}^k + w_{i,j}^k\left(x_j\left|\frac{\partial R}{\partial z}\right|_i^k + \left|\frac{\partial R_2}{\partial z}\right|_i^k\right)\right]\left|\frac{\partial w}{\partial x}\right|_{i,j}^k - w_{i,j}^k\left|\frac{\partial w}{\partial z}\right|_{i,j}^k + \frac{1+K}{\alpha^2}\left[\frac{1}{(R_i^k)^2}\left[1 + \left(x_j\left|\frac{\partial R}{\partial z}\right|_i^k + \left|\frac{\partial R_2}{\partial z}\right|_i^k\right)^2\right]\left|\frac{\partial^2 w}{\partial x^2}\right|_{i,j}^k - \frac{2}{R_i^k}\left(x_j\left|\frac{\partial R}{\partial z}\right|_i^k + \left|\frac{\partial R_2}{\partial z}\right|_i^k\right)\left|\frac{\partial^2 w}{\partial x \partial z}\right|_{i,j}^k + \left|\frac{\partial^2 w}{\partial z^2}\right|_{i,j}^k + \frac{1}{R_i^k}\left[\frac{1}{x_j R_i^k + R_{2i}^k} + \frac{2}{R_i^k}\left(x_j\left|\frac{\partial R}{\partial z}\right|_i^k + \left|\frac{\partial R_2}{\partial z}\right|_i^k\right)\left|\frac{\partial R}{\partial z}\right|_i^k - \left(x_j\left|\frac{\partial^2 R}{\partial z^2}\right|_i^k + \left|\frac{\partial^2 R_2}{\partial z^2}\right|_i^k\right)\right]\left|\frac{\partial w}{\partial x}\right|_{i,j}^k + \frac{K}{\alpha^2}\left(\frac{1}{R_i^k}\left|\frac{\partial \omega}{\partial x}\right|_{i,j}^k + \frac{\omega_{i,j}^k}{x_j R_i^k + R_{2i}^k}\right) - G\cos\theta \quad (36)$$

$$\omega_{i,j}^{k+1} = \omega_{i,j}^{k} + \Delta t\left\{\frac{1}{R_i^k}\left[x_j\left|\frac{\partial R}{\partial z}\right|_i^k + \left|\frac{\partial R_2}{\partial z}\right|_i^k - u_{i,j}^k + w_{i,j}^k\left(x_j\left|\frac{\partial R}{\partial z}\right|_i^k + \left|\frac{\partial R_2}{\partial z}\right|_i^k\right)\right]\left|\frac{\partial \omega}{\partial x}\right|_{i,j}^k - w_{i,j}^k\left|\frac{\partial \omega}{\partial z}\right|_{i,j}^k - \frac{K}{\alpha^2 J}\left[2\omega_{i,j}^k + \frac{1}{R_i^k}\left|\frac{\partial w}{\partial x}\right|_{i,j}^k - \left|\frac{\partial u}{\partial z}\right|_{i,j}^k + \frac{1}{R_i^k}\left(x_j\left|\frac{\partial R}{\partial z}\right|_i^k + \left|\frac{\partial R_2}{\partial z}\right|_i^k\right)\left|\frac{\partial u}{\partial x}\right|_{i,j}^k\right] + \frac{M}{\alpha^2 J}\left[-\frac{\omega_{i,j}^k}{(x_j R_i^k + R_{2i}^k)^2} + \frac{1}{(R_i^k)^2}\left(1 + \left(x_j\left|\frac{\partial R}{\partial z}\right|_i^k + \left|\frac{\partial R_2}{\partial z}\right|_i^k\right)^2\right)\left|\frac{\partial^2 \omega}{\partial x^2}\right|_{i,j}^k + \left|\frac{\partial^2 \omega}{\partial z^2}\right|_{i,j}^k - \frac{2}{R_i^k}\left(x_j\left|\frac{\partial R}{\partial z}\right|_i^k + \left|\frac{\partial R_2}{\partial z}\right|_i^k\right)\left|\frac{\partial^2 \omega}{\partial x \partial z}\right|_{i,j}^k + \frac{1}{R_i^k}\left[\frac{1}{x_j R_i^k + R_{2i}^k} + \frac{2}{R_i^k}\left(x_j\left|\frac{\partial R}{\partial z}\right|_i^k + \left|\frac{\partial R_2}{\partial z}\right|_i^k\right)\left|\frac{\partial R}{\partial z}\right|_i^k - \left(x_j\left|\frac{\partial^2 R}{\partial z^2}\right|_i^k + \left|\frac{\partial^2 R_2}{\partial z^2}\right|_i^k\right)\right]\left|\frac{\partial w}{\partial x}\right|_{i,j}^k\right]\right\} \quad (37)$$

$$u_{i,j}^k = \left(\frac{R_{2i}^k}{x_j R_i^k + R_{2i}^k}\right)u_{i,1}^k + \left(x_j\left|\frac{\partial R}{\partial z}\right|_i^k + \left|\frac{\partial R_2}{\partial z}\right|_i^k\right)w_{i,j}^k + \frac{x_j^2(2-x_j^2)}{x_j R_i^k + R_{2i}^k}\left[R_{1i}^k\alpha_0\left|\frac{\partial R_1}{\partial t}\right|_i^k - R_{2i}^k u_{i,1}^k\right] \quad (38)$$

The prescribed boundary and initial conditions (28) to (31) throughout the bifurcated artery segment are approximated by finite difference scheme as follow.

$$u_{i,j}^1 = w_{i,j}^1 = \omega_{i,j}^1 = 0 \quad (39)$$

$$u_{i,1}^k = 0 \text{ and } w_{i,2}^k = w_{i,1}^k \text{ for } z \le z_3 \quad (40)$$

$$u_{i,1}^k = \alpha_0\left|\frac{\partial R_2}{\partial t}\right|_i^k \text{ and } w_i^k = 0 \text{ for } z \ge z_3 \quad (41)$$

$$u_{i,N+1}^k = \alpha_0\left|\frac{\partial R_1}{\partial t}\right|_i^k \text{ and } w_{i,N+1}^k = 0 \quad (42)$$

A thorough stability criterion combined from Markham and Proctor (1983) and Hirt (1968) is implemented. For the current method of solution, uniform steps of z and x are used. Hence the computational calculation is sufficiently stable with criterion:

$$\Delta t^k \le min\left[\frac{\Delta z}{|w_{i,j}^k|}, \frac{\Delta x}{|u_{i,j}^k|}\right] \quad (43)$$

In the numerical algorithm for the current case, the time interval is prescribed to be $dt = 0.0001$. The results converge pleasantly with error at order $\approx 10^{-4}$.

6. Results and discussions

In order to perform the computations according to major physiological implications, the imposed parameters and quantities are:

$\rho = 1.06 \times 10^3 kg/m^3$; $\omega_p = 2\pi f_p$; $f_p = 1.2Hz$;
$\phi = 0°$; $a = 1$; $d' = 5$; $l_0 = 10$; $r_1 = 0.7a$; $\tau_m = 0.48$;
$z_{max} = 50$; $z_1 = 30$; $\theta = 30°$; $U_0 = 0.5$

In this study, the results are taken at dimensionless time $t = 30$ to ensure the steadiness. The uniform non-staggerred grid of finite difference is set to have $\Delta z = 0.1$ and $\Delta x = 0.025$. The dimensionless quantities for micropolar fluid model are taken to be $K = 0.1$, $M = 0.1$, $J = 0.1$ and $\alpha = 5$ where choices of the values are adopted from Abdullah and Amin (2010). K expresses the ratio of micropolar viscosity coefficient to fluid viscosity coefficient, where the inequality $2\mu + \kappa \ge 0$ and $\kappa \ge 0$ must be satisfied. Hence the value should be $K \ge -2$. K represents the polar effect between blood corpuscles and fluid. Besides, M means the microstructure size effect parameter, which represents the ratio of corpuscle to radius of the annulated region (Abdullah and Amin, 2010). Parameter M consists of a dimensional parameter γ which occurs in Eq. 37 as coefficient of gyro-viscosity in this micropolar model. On the other hand, parameter J is the dimensionless form of the micro-inertia coefficient. Muthu et al. (2003) pointed out that this coefficient is insignificantly small, hence

may be neglected from the governing equation system. However, some other previous researches appoint a very small value onto it. The Womersley number is implicated to represent pulsatility of blood and conditions of the blood vessel. According to Womersley (1955), choices of the dimensionless value roughly vary from 0 to 10 for animals, depend essentially on vessel size and pulse rate. Also, a dimensionless parameter G is introduced to describe the condition of external body force, where gravitational acceleration is involved in this study. G is directly proportional to gravitational acceleration. In this study, values of G are chosen to be 0.01, 0.1 and 0.2.

Numerical validation is done by comparing results with Abdullah and Amin (2010) who studied micropolar fluid flow through a straight tapered artery with mild stenosis. Fig. 3 presents axial velocity profiles along x under different conditions of gravity at the parent artery. Also, the axial velocity profiles are taken at the centre of the axisymmetrical trunk where $x = 33$. From the figure, when the gravitational acceleration is ignored, the current model shows good agreement with Abdullah and Amin (2010). The graphs are noticed to be decreasing from their individual maximums and finally become zero at the vessel wall as prescribed in the boundary conditions. As G increases, the individual maxima of each axial velocity line decreases. The expression is also described by a cosine function of time which involves the heart action. However, expression of G is not altered by time and hence remains the same throughout a complete calculation. From this graph, one can conclude that the additional term of external body force is significant in determining hemodynamic and nature of blood flow.

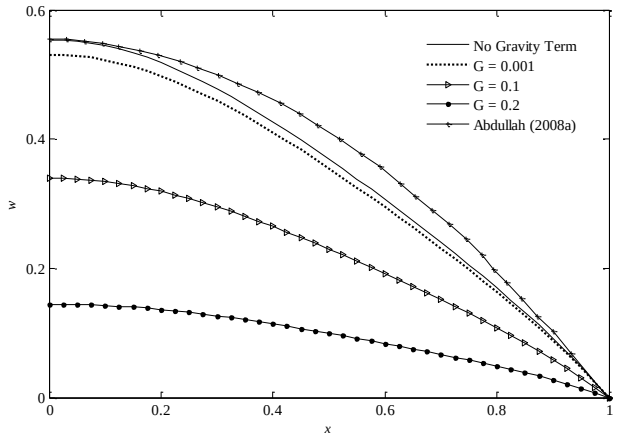

Fig. 3: Axial velocity at the parent artery
($J = 0.1, M = 0.1, K = 0.1, \alpha = 5, z = 12$)

Fig. 4 shows axial velocity profiles along the dimensionless radial direction under different values of G at the daughter artery. The location is taken at $z = 34$, which is right after the bifurcated junction. The velocities start from zero at the inner wall as determined as the boundary conditions. Each curve is then increases until its individual maxima near the centre of artery, and then drops gradually to zero at the outer wall. No negative velocity is observed along the segment, thus no flow separation takes place for these cases. This may be considered as stenosis mildness and bifurcation angle of the daughter branches, which has been discussed by Chakravarty and Mandal (1997), where by wider angle of the bifurcation yields higher maximum of axial velocity at the apex of daughter branch.

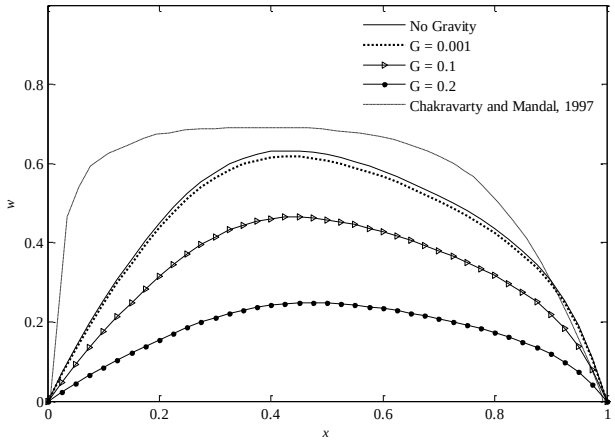

Fig. 4: Axial velocity at daughter artery
($J = 0.1, M = 0.1, K = 0.1, \alpha = 5, z = 34$)

Next, Fig. 5 and Fig. 6 show axial velocity profiles at different axial positions. They possess the same parameters values except for the external gravity force G, which is set to be $G = 0.01$ and $G = 0.02$ respectively. Generally, these two graphs exhibit similar patterns, despite the velocities under higher gravitational acceleration yield relatively lower maximum values. Velocities at the upstream $z = 8$ and downstream ($z = 31$) of parent branch remain close values, with slightly higher velocity at the downstream which is near to the bifurcation junction (flow steadiness after the constriction region is re-obtained). When passes through stenosis peak at $z = 15$, the maximum velocity drops; then right after the stenosis ($z = 20$), it rises back to a value which is still lower than the upstream. After getting steadier velocity at $z = 31$, the axial velocity continues to rise until reaching the entrance of branching junction at $z = 32$. Upon reaching the daughter branch, axial velocity for this graph is computed from the inner wall as $x = 0$ to the outer wall $x = 1$. At the frontal part of daughter branch, velocity maximum is observed near the middle, and then drops gradually to zero at vessel wall. But at posterior part of the daughter segment, velocity rises gradually from zero at the inner wall to reach its maximum near the outer vessel wall, and then drops drastically to zero upon reaching the outer wall. The expression of dimensionless G is directly proportional to vessel size and gravity acceleration. Hence, lower value of G can represent a condition of microgravity. Thus, is can also be concluded that under lower gravity condition, blood velocity gets higher. Apart from heart healthiness issue which is not discussed here by mean of mathematical

modelling, the main reason affecting flow velocity is blood pressure. Since pressure parameter is not included in the computational method for this problem, we may only roughly adjudge that blood pressure under lower gravity conditions is lower.

Fig. 7 and Fig. 8 present the axial velocity profiles across x for the parent and daughter branch respectively, under the condition of G = 0.2 with different values of K. As discussed above, K is defined by ratio of the dynamic microrotation viscosity to the dynamic Newtonian viscosity of fluid. From the momentum equations, once the microrotation viscosity coefficient is set to be zero, the conservation of linear momentum is then free from microstructure, i.e. becomes the classical Newtonian Navier-Stokes equations. Therefore, the dynamic microrotation viscosity is also a measurement to determine how deviated a model is from the common Navier-Stokes model (Lukaszewicz, 1999). Also, in context of blood suspension, higher value of κ indicates greater polar effects of microstructures. From both Fig. 7 and Fig. 8, greater value of K yields lower maximum velocity. This shows that axial velocity is notably influenced by microrotation of suspended microstructures in blood. On the other hand when comparing between the two figures, velocity at daughter branch is generally higher than the parent branch.

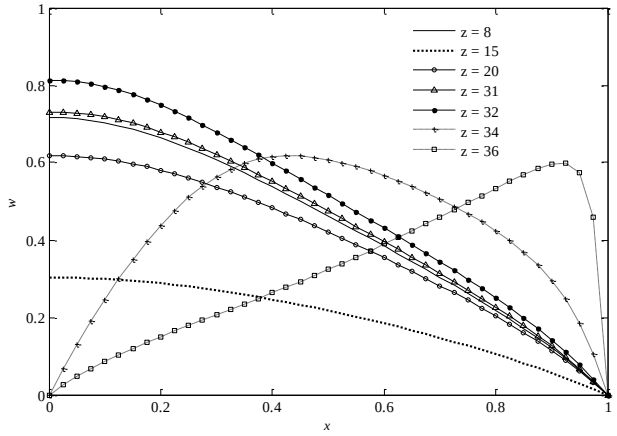

Fig. 5: Axial Velocity at Different z positions at t = 30 (G = 0.01, J = 0.1, M = 0.1, K = 0.1, α = 5)

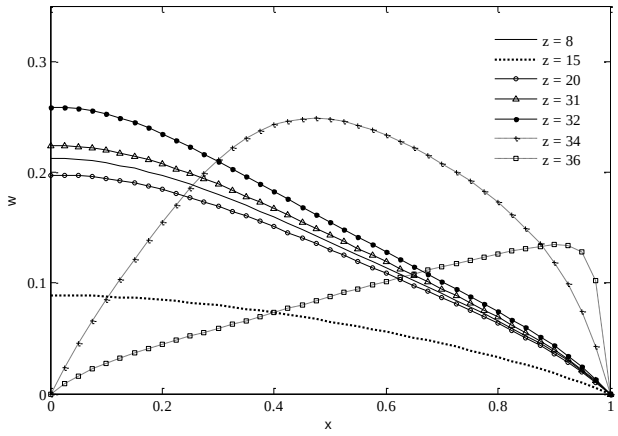

Fig. 6: Axial velocity at different z positions at t = 30 (G = 0.2, J = 0.1, M = 0.1, K = 0.1, α = 5)

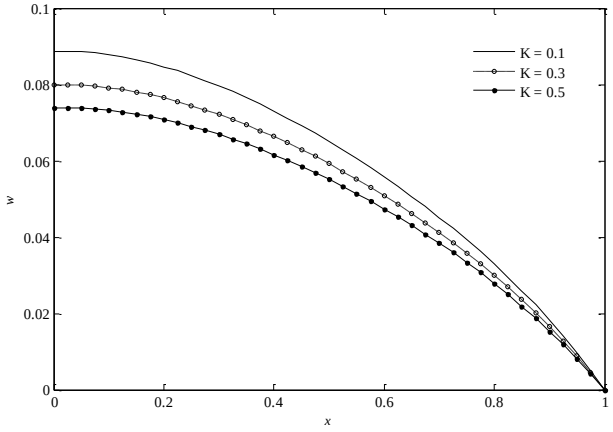

Fig. 7: Axial velocity with different values of K at the parent branch with Mild stenosis (t = 30, G = 0.2, J = 0.1, M = 0.1, α = 5, z = 15)

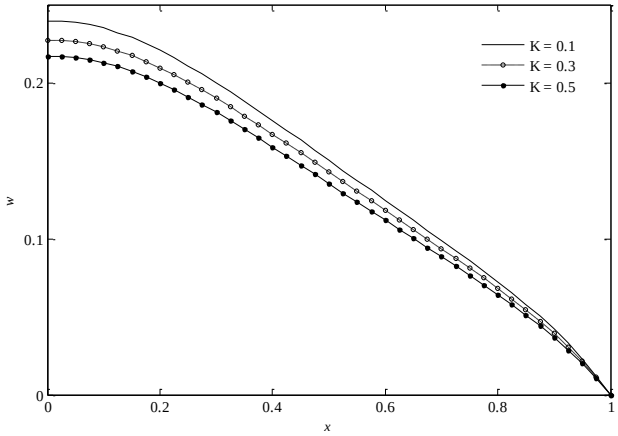

Fig. 8: Axial velocity with different values of K at bifurcated junction (t = 30, G = 0.2, J = 0.1, M = 0.1, α = 5, z = 31.5)

Fig. 9 and Fig. 10 show angular velocity profiles across x for the parent and daughter branch respectively, under variation of gravitational acceleration. Angular velocity without considering gravitational acceleration is higher than all other conditions at both parent and daughter branches. As gravity force increases, the velocity decreases. However when value of K increases, angular velocity also increases under same value of gravity acceleration.

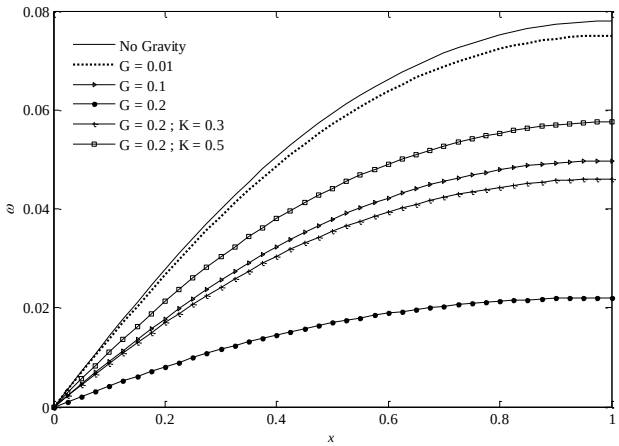

Fig. 9: Angular velocity profiles at parent branch measured at stenosis peak

(t = 30, J = 0.1, M = 0.1, α = 5, z = 15)

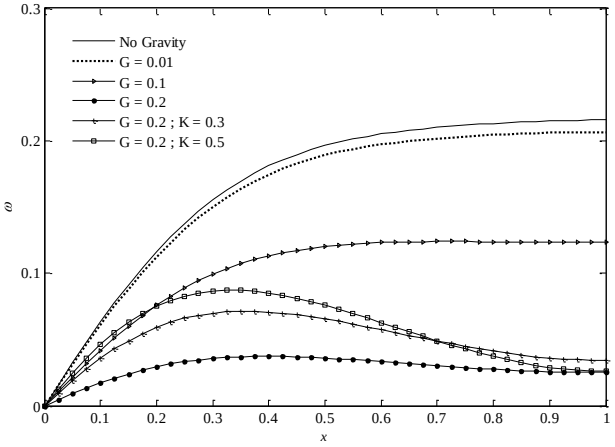

Fig. 10: Angular velocity profiles at bifurcated junction (t = 30, J = 0.1, M = 0.1, α = 5, z = 31.5)

Fig. 11 and Fig. 12 present variation of dimensionless wall shear stress of outer wall along the parent artery and daughter artery respectively. Each figure compares wall shear stress under different values of dimensionless gravity parameter G, and also under different values of micropolar model viscosity ratio K. At the parent artery as shown in Fig. 11, maximum magnitude of wall shear stress occurs acutely at the beginning of stenosis. And then, it drops gradually until a minimum magnitude. According to blood flow nature, a slight distortion occurs here. The shear stress is then rises again upon reaching the non-constricted parent trunk. At the parent artery, wall shear stress remains negative magnitude. At the entrance of bifurcation branch near z = 30, wall shear stress starts to drop again. But it immediately rises back to positive values, as shown in Fig. 12. Among the graphs, it is noticed that with increment of G, magnitude of wall shear stress also increases. However, these changes are too tiny thus insignificant for flow separations to occur. Further, when comparing effects of different values of K, lower K yields lower starting magnitude of wall shear stress. Despite, it fluctuates more, which grants higher maximum and lower minimum at the stenotic region, as well as the posterior segment of parent branch. At the junction of bifurcation, higher value of K causes wall shear stress to drop more compared to others. But, as the flow get steadier along the daughter branch, higher value of K yields higher value of wall shear stress along the outer wall.

Fig. 13 shows wall shear stress distribution along the inner wall of daughter branch. This graph exhibits good agreement with previous research done by Lou and Yang (1993). The graph remains at positive magnitude throughout the segment for every case. Drastic increment and decrement happen near the bifurcated junction, and then it is maintained gradually. Generally, magnitude of inner wall shear stress gets lower when the gravity parameter gets higher. This is observed to be opposite from the outer wall shear stress. Besides, under higher values of K, the curve yields higher magnitude throughout the inner wall.

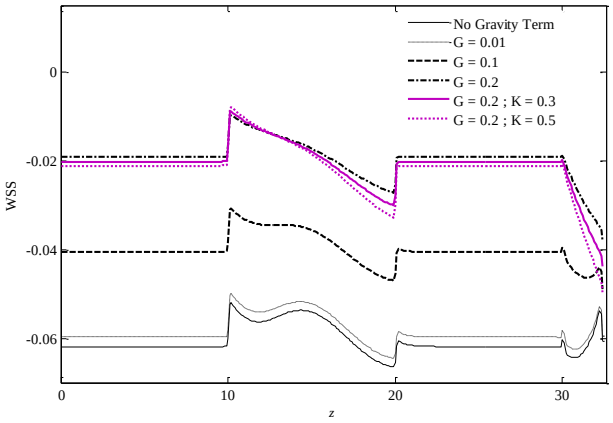

Fig. 11: Dimensionless wall shear stress distributions along the parent artery (J = 0.1, M = 0.1, K = 0.1, α = 5)

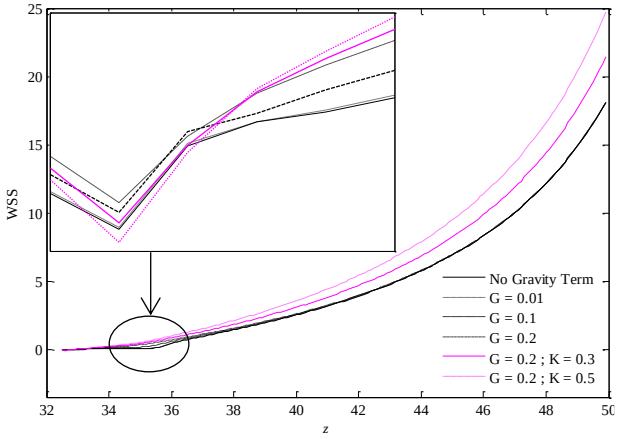

Fig. 12: Dimensionless wall shear stress for outer wall along the daughter brach (J = 0.1, M = 0.1, K = 0.1, α = 5)

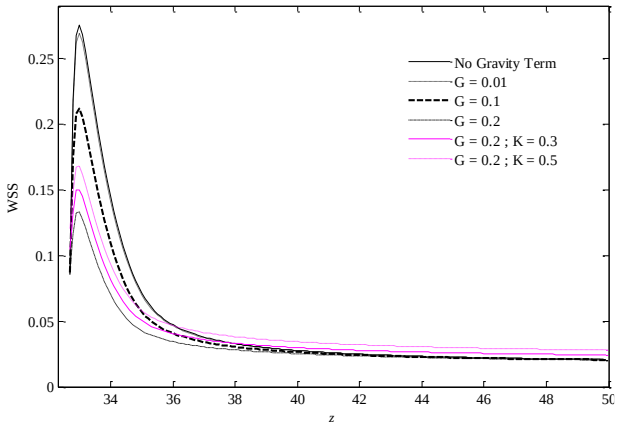

Fig. 13: Dimensionless wall shear stress for inner wall along the daughter brach (J = 0.1, M = 0.1, K = 0.1, α = 5)

7. Conclusion

A micropolar fluid flow model passes through an artery bifurcation under the effects of gravitational acceleration is studied. Three main aspects are included in the study, which is geometrical structure

of vessel segment, micropolar fluid behaviour, and the effects of additional gravity vector on axial momentum. The dimensionless values of difference in maximum wall shear stress and velocities are not more than ~0.5. Hence, the significance is relatively low. Remarkable influences are noticed along with different values of gravity parameter. From the numerical results, increment of dimensionless gravity parameter value yields lower axial velocity along the bifurcation segment. Also, increment of gravity yields higher magnitude of outer wall shear stress and lower magnitude of inner wall shear stress. Further, increment of K value yields lower axial velocity; lower wall shear stress at both outer and inner walls, but with greater fluctuations. At the branching junction, distortion happens which could lead to various consequences such as multiple stenosis. For future researches, gravitational terms shall always be considered in the governing equations. Further studies on different non-Newtonian models of blood flow through bifurcated artery will also be carried out. Besides, future studies may consider blood pressure gradient as one of the parameters to be measured instead of using a prescribed function.

References

Abdullah I and Amin N (2010). A micropolar fluid model of blood flow through a tapered artery with a stenosis. Mathematical Methods in the Applied Sciences, 33(16): 1910-1923.

Ariman TMAND, Turk MA, and Sylvester ND (1973). Microcontinuum fluid mechanics: A review. International Journal of Engineering Science, 11(8): 905-930.

Burrowes KS and Tawhai MH (2006). Computational predictions of pulmonary blood flow gradients: gravity versus structure. Respiratory Physiology and Neurobiology, 154(3): 515-523.

Burrowes KS, Hunter PJ, and Tawhai MH (2005). Investigation of the relative effects of vascular branching structure and gravity on pulmonary arterial blood flow heterogeneity via an image-based computational model. Academic Radiology, 12(11): 1464-1474.

Burton AC (1966). Introductory text: Physiology and biophysics of the circulation. Book Medical Publisher, Chicago, Illinois, USA.

Chakravarty S and Mandal PK (1997). An analysis of pulsatile flow in a model aortic bifurcation. International Journal of Engineering Science, 35(4): 409-422.

Chakravarty S and Mandal PK (2013). Heat transfer to micropolar fluid flowing through an irregular arterial constriction. International Journal of Heat and Mass Transfer, 56(1-2): 538-551.

Chakravarty S and Sen S (2005). Dynamic response of heat and mass transfer in blood flow through stenosed bifurcated arteries. Korea-Australia Rheology Journal, 17(2): 47-62.

Chakravarty S, Datta A, and Mandal PK (1996). Effect of body acceleration on unsteady flow of blood past a time-dependent arterial stenosis. Mathematical and Computer Modelling, 24(2): 57-74.

Devanathan R and Parvathamma S (1983). Flow of micropolar fluid through a tube with stenosis. Medical and Biological Engineering and Computing, 21(4): 438-445.

Eringen AC (1966). Theory of micropolar fluids. Journal of Mathematics and Mechanics, 16(1): 1-18.

Ghosh BC (1986). Motion under gravity of a micropolar viscous fluid contained between two inclined planes. Proceedings of the Indian National Science Academy, 53A(6): 760-767.

Hirt CW (1968). Heuristic stability theory for finite-difference equations. Journal of Computational Physics, 2(4): 339-355.

Ikbal MA, Chakravarty S, and Mandal PK (2011). Numerical simulation of mass transfer to micropolar fluid flow past a stenosed artery. International Journal for Numerical Methods in Fluids, 67(11): 1655-1676.

Ku DN (1997). Blood flow in arteries. Annual Review of Fluid Mechanics, 29(1): 399-434.

Lou Z and Yang WJ (1993). A computer simulation of the non-Newtonian blood flow at the aortic bifurcation. Journal of Biomechanics, 26(1): 37-49.

Lukaszewicz G (1999). Micropolar fluids: Theory and applications. Springer Science and Business Media, Birkhauser Boston, New York, USA.

Markham G and Proctor MV (1983). Modifications to the two-dimensional incompressible fluid flow code ZUNI to provide enhanced performance. C.E.G.B. report TPRD/L/0063/M82, London, UK.

Muthu P, Kumar BR, and Chandra P (2003). Effect of elastic wall motion on oscillatory flow of micropolar fluid in an annular tube. Archive of Applied Mechanics, 73(7): 481-494.

Olufsen MS, Ottesen JT, Tran HT, Ellwein LM, Lipsitz LA, and Novak V (2005). Blood pressure and blood flow variation during postural change from sitting to standing: Model development and validation. Journal of Applied Physiology, 99(4): 1523-1537.

Payne SJ (2004). Analysis of the effects of gravity and wall thickness in a model of blood flow through axisymmetric vessels. Medical and Biological Engineering and Computing, 42(6): 799-806.

Shaw S, Gorla RSR, Murthy PVSN, and Ng CO (2009). Pulsatile Casson fluid flow through a stenosed bifurcated artery. International Journal of Fluid Mechanics Research, 36(1): 43-63.

Tan YB, Mustapha N, and Sarifuddin (2014). Blood flow through a stenosed artery bifurcation under the effects of gravity. In the AIP Conference Proceedings, AIP, 1635(1): 241-248. https://doi.org/10.1063/1.4903590

Womersley JR (1955). Method for the calculation of velocity, rate of flow and viscous drag in arteries when the pressure gradient is known. The Journal of Physiology, 127(3): 553-563.